HORIZON 2020 PROGRAMME – TOPIC H2020-LC-BAT-14-2020

Self-healing functionalities for long lasting battery cell chemistries

Research and Innovation Action (RIA)

BAT4EVER

Autonomous Polymer based Self-Healing Components for high performant LIBs

Grant Agreement No. 957225

Starting date: 1 September 2020 – Duration: 42 months

Deliverable D4.6

Report on macroscale Multiphysics modelling of cell components

DOCUMENT INFORMATION

Deliverable number	D4.6
Deliverable title	Report on macroscale Multiphysics modelling of cell components
Work Package	WP4
Deliverable type	Report
Dissemination level	Public
Due date	30.11.2023 (M39)
Pages	25
Document version	4.0
Lead author(s)	Kato Daems, Vrije Universiteit Brussel (VUB) Emre Guney, Enwair Enerji Teknolojileri Anonimsirketi (ENW)

DOCUMENT CHANGE HISTORY

Version	Date	Author	Description
DRAFT			
0.1	15/01/2024	Kato Daems, Vrije Universiteit Brussel (VUB)	Creation
0.2	30/01/2024	Emre Guney, Enwair Enerji Teknolojileri Anonimsirketi (ENW)	Input contributions parametrization experiments
0.3	15/02/2024	Kato Daems, Vrije Universiteit Brussel (VUB)	Input modeling results
FIRST PEER REVIEW			
1.1	16/02/2024	Anja Marinow, Martin-Luther-Universitaet Halle-Wittenberg, MLU	Proofreading and peer review
1.2	21/02/2024	Boyan Iliev, IOLITEC Ionic Liquids Technologies GMBH	Proofreading and peer review
SECOND PEER REVIEW			
2.0	23.02.2024	Dr. Anja Marinow, Martin-Luther-University Halle-Wittenberg (MLU) Dr. Boyan Iliev, Iolitec Ionic Liquids Technologies GMBH (IOL)	Second peer review
2.1	23.02.2024	Kato Daems, Vrije Universiteit Brussel (VUB)	Consolidation of input from reviewers
COORDINATOR APPROVAL			
3.0	27.02.2024	Dr. K. Burak Dermenci, Vrije Universiteit Brussel (VUB)	Coordinator review and approval
FINAL VERSION			
4.0	27.02.2024	Ines Boursot, Vrije Universiteit Brussel (VUB)	Format review, version ready for submission

ABSTRACT FOR DISSEMINATION

Abstract

The development time of new lithium-ion battery compositions can be significantly reduced by applying electrochemical models to predict the performance of the battery and to optimize the components to obtain enhanced performance. The Doyle-Fuller-Newman pseudo-2-dimensional model is used to set up the theoretical modeling framework. The accuracy of the model is dependent on the characterization of the parameters describing the electrolyte and electrodes. This deliverable (D.4.6) summarizes the theoretical framework of the electrochemical model and the parametrization experiments executed for this task, including the validation of the model with experimental results.

TABLE OF CONTENTS

LIST OF PARTNERS

No	Logo	Name	Short Name	Country	Project entry date	Project exit date
1		VRIJE UNIVERSITEIT BRUSSEL	VUB	Belgium		
2		ENWAIR ENERJI TEKNOLOJILERI ANONIMSIRKETI	ENW	Turkey		
3		MARTIN-LUTHER-UNIVERSITAET HALLE-WITTENBERG	MLU	Germany		
4		DEUTSCHES ZENTRUM FUER LUFT - UND RAUMFAHRT EV	DLR	Germany		
5		IOLITEC IONIC LIQUIDS TECHNOLOGIES GMBH	IOLITEC GmbH	Germany		
6		UNIVERSIDAD COMPLUTENSE DE MADRID	UCM	Spain		
7		UNIVERSITA DEGLI STUDI DI MODENA E REGGIO EMILIA	UNIMORE	Italy		
8		VESTEL ELEKTRONIK SANAYI VE TICARET ANONIM SIRKETI	VEL	Turkey		
9		CLEANCARB SARL	CCB	Luxembourg		
11		FAAM RESEARCH CENTER SRL	FRC	Italy	01/09/2020	The day after notification of termination

ABBREVIATIONS

Acronym	Description
Al	Aluminium (positive current collector)
Cu	Copper (negative current collector)
RT	Room Temperature
IL	Ionic Liquid: N-methylpyrrolidinium bis(fluoromethanesulfonyl)imide (1.3 M LiTFSI-PYR_{14}TFSI)
GF	Glass Fiber
Si-SH	Self-healing silicon anode active material
SS	Stainless steel blocking electrodes
NMC811-SH	Self-healing $LiNi_{0.8}Mn_{0.1}Co_{0.1}O_2$ cathode active material
OCP	Open Circuit Potential
DFN	Doyle-Fuller-Newman
P2D	Pseudo-2-dimensional
PDE	Partial differential equation
RMSE	Root-mean-square error

LIST OF FIGURES

LIST OF TABLES

EXECUTIVE SUMMARY

Developing novel battery chemistries require testing of and optimizing the battery components to obtain the desired performance for a certain application. Testing and optimizing battery components are time consuming steps. In order to reduce developing time electrochemical modeling can be useful to predict the performance of the components and the battery system. The electrochemical model can help to understand the mechanisms driving the Li-ion battery. The bottleneck of electrochemical modeling is the parametrization of the battery components, since only an accurate simulation can be obtained when parameters close to the system are inserted in the model. Therefore, this deliverable consists of two parts. The first part focuses on the development of the electrochemical model, starting from a monolayer pouch cell and upscaling towards 500 mAh multilayered pouch cells, including the parametrization experiments to obtain an accurate model. The second part contains the validation of the electrochemical model with experimental results, followed by an optimization of the battery components by varying some parameters.

1. INTRODUCTION

BAT4EVER project considers the development of self-healing battery components, battery assembly and testing in a comprehensive way.

Nowadays, the advancement and refinement of batteries rely on experimental trial-and-error methods, resulting in notably expensive and time-intensive development processes. Introducing electrochemical models for the design, optimization, and performance prediction of emerging battery technologies holds the potential to significantly shorten development timelines.[1] This modeling approach serves as a valuable tool for comprehending, refining, and forecasting the intricate interactions among essential processes occurring at the interfaces of electrolyte and electrodes. To delve into the complex interplay of chemical reactions and charge transport phenomena within the electrodes, a comprehensive theoretical framework is essential. This framework aids in achieving a deeper understanding of the mechanisms that govern the behaviour of lithium-ion batteries across diverse operational conditions.

The input parameters of the model play a crucial role in order to obtain accurate simulations of the battery performance. Therefore the characterization of the used battery components is required and is thought to be the bottleneck of electrochemical modeling because over 30 input parameters are needed. The parameters include geometrical, electrochemical and kinetic parameters, e.g. thickness of the battery components, diffusion coefficient and exchange current density. The full list of required parameters, and there values, is presented in Table 3.[2]

2. DEVELOPMENT OF AN ELECTROCHEMICAL MODEL FOR MONOLAYER POUCH CELLS

In this section, an overview on the macroscale modelling activities for the BAT4EVER project at the VUB is given. An isothermal pseudo-2-dimensional (P2D) framework based on the Doyle-Fuller-Newman (DFN) model was used to assess the performance of monolayer and an 500 mAh multilayer pouch cells.

2.1 THEORETICAL FRAMEWORK

The P2D model is governed by four non-linear partial differential equations (PDE) describing charge- and mass conservations in both the electrolyte and electrode phases, combined with one algebraic equation, i.e., the Butler-Volmer equation describing the electrode kinetics of the intercalation and de-intercalation reactions at the electrode-electrolyte interfaces.[3–6] The boundary conditions applied in the DFN model describe the electric ground, application of current and the continuity of flux across each boundary.[1,7] The governing equations and applicable boundary conditions are presented in Table 1.

To reduce the computational burden of the P2D model assumptions are being applied.[2,8] The modeling framework uses the concentrated solution theory to describe the transport characteristics of the electrolyte, assuming that the electrolyte consists of a binary Li-salt in a single solvent. In the solid electrode phase, the porous electrode theory is applied to simulate the composite electrodes.[2,5,9] The composite electrodes consist of electrolyte, solid active materials, conductive fillers and binders. The active material particles in the electrodes are assumed to be identical spherical particles that are uniformly distributed within the electrodes.[2,6] However, in practice electrodes consist of non-spherical particles, exhibit large dispersity, and porosity and volume fraction changes, crack formation, lithium plating and stripping and stress effects during battery cycling. Therefore, the accuracy of the P2D model is limited for predicting cell behaviour under extreme operating conditions.[1,2]

The governing equations and their boundary conditions are implemented in the COMSOL Multiphysics Software, which linearizes and numerically solves them simultaneously.[9] The accuracy of the electrochemical model relies on the precise characterization of approximately 30 material and electrochemical parameters, presented in Table 3. Component analysis is time-consuming and requires specific measurement techniques, consequently being the bottleneck for modeling purposes.[2,10]

Table 1: Governing equations and the applied boundary conditions in the P2D electrochemical modeling framework.

	Governing equation	Boundary conditions	
Mass conservation electrode	$\frac{\partial c_s}{\partial t} = \frac{1}{r^2}\frac{\partial}{\partial r}\left(r^2 D_s \frac{\partial c_s}{\partial r}\right)$	$\left.\frac{\partial c_s}{\partial r}\right\|_{r=0} = 0$ $-D_s \left.\frac{\partial c_s}{\partial r}\right\|_{r=R_s} = \frac{j_{Li}}{a_s F}$	(1)
Mass conservation electrolyte	$\frac{\partial(\varepsilon_e c_e)}{\partial t} = \nabla \cdot \left(D_e^{eff} \nabla c_e\right) + \frac{1-t^+}{F} j_{Li} - \frac{i_e \cdot \nabla t^+}{F}$	$\left.\frac{\partial c_l}{\partial x}\right\|_{x=L_{neg}+L_{sep}+L_{pos}} = \left.\frac{\partial c_l}{\partial x}\right\|_{x=0} = 0$	(2)
Charge conservation electrode	$\nabla \cdot \left(\sigma^{eff} \nabla \phi_s\right) - j_{Li} = 0$	$\left.\frac{\partial \phi_s}{\partial x}\right\|_{x=0} = -\frac{I_{app}}{A_{surf}\sigma^{eff}}$ $\left.\frac{\partial \phi_s}{\partial x}\right\|_{x=L_{neg}+L_{sep}} = 0$ $\left.\frac{\partial \phi_s}{\partial x}\right\|_{x=L_{neg}+L_{sep}} = 0$ $\left.\frac{\partial \phi_s}{\partial x}\right\|_{x=L_{neg}+L_{sep}+L_{pos}} = -\frac{I_{app}}{A_{surf}\sigma^{eff}}$	(3)
Charge conservation electrolyte	$\nabla \cdot \left(\kappa^{eff} \nabla \phi_e\right) + \nabla \cdot \left(\kappa_D^{eff} \nabla \ln c_e\right) + j_{Li} = 0$	$\left.\frac{\partial \phi_e}{\partial x}\right\|_{x=L_{neg}+L_{sep}+L_{pos}} = \left.\frac{\partial \phi_e}{\partial x}\right\|_{x=0} = 0$	(4)
Butler-Volmer kinetics	$j_{Li} = i_0\left[\exp\left(\frac{\alpha_a F}{RT}\eta\right) - \exp\left(-\frac{\alpha_c F}{RT}\eta\right)\right]$		(5)
Exchange current density	$i_0 = k(c_e)^{\alpha_a}\left(c_{s,max} - c_s\right)^{\alpha_c}(c_s)^{\alpha_c}$		(6)
Overpotential of reaction	$\eta = \phi_s - \phi_e - U_{eq} - iR$		(7)

Where: D_s = Li-ion diffusion coefficient of the electrode active material, a_s = specific interfacial area, F = Faraday's constant, ε_e = volume fraction of the electrolyte, $D_e^{eff} = D_e \varepsilon_e^{brugg}$ = the

effective salt diffusion coefficient in the electrolyte, D_e = diffusion coefficient in the electrolyte, $\varepsilon^{brugg}{}_e$ = the Bruggeman porosity exponent, t^+ = the Li-ion transference number of the electrolyte, $\sigma^{eff} = \varepsilon_s\sigma$ = the effective conductivity in the solid electrode, σ = electrical conductivity of the active solid material, I_{app} = the applied (dis)charge current, A_{surf} = the electrode plate area, $\kappa^{eff} = \kappa\varepsilon_e^{brugg}$ = the effective ionic conductivity of the electrolyte, α_a = the anodic transfer coefficient, α_c = the cathodic transfer coefficient, R = the universal gas constant, T = the temperature, k = the kinetic rate constant, $c_{s,max}$ = the maximum lithium concentration in the electrode, U_{eq} = the open circuit potential, and iR = the Ohmic losses.[1,2,5,7]

The starting point of the electrochemical model is a P2D isothermal model on monolayer pouch cell level, the geometry constructed contains five sublayers of Cu-foil, Si-SH anode active material, separator, NMC811-SH cathode active material, and Al-foil as shown in Figure 1a. After optimization and experimental validation, the model geometry is expanded to 140 mAh and 500 mAh pouch cells by stacking the cell components to obtain a geometry as depicted in Figure 1b.

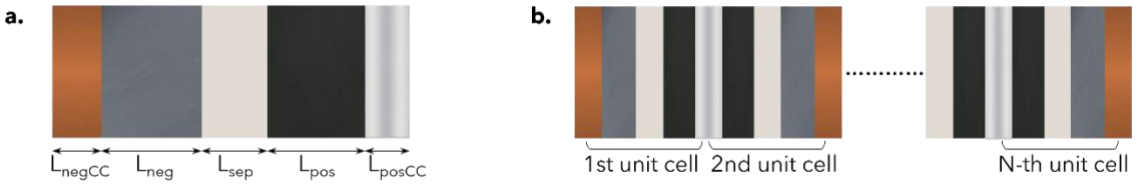

Figure 1: Geometry of the P2D electrochemical model at a. monolayer pouch cell level and b. at multilayer pouch cell level (where the 140 mAh pouch cell contains 3 layers of Si-SH and 3 layers of NMC811-SH; and the 500 mAh pouch cell consists out of 12 Si-SH layers and 11 NMC811-SH layers)

2.2 MODEL VALIDATION

The modeling frameworks is validated by experimental charge/discharge tests. Manufactured cells are first subjected to 5 formation cycles at 0.02C under CCCV conditions (I<0.05C). The charge/discharge cycling of the cells is carried out at C/10 at RT in a 2.7-4.2 V operating voltage window.

3. SUMMARY OF PARAMETRIZATION TESTS PERFORMED ON NMC811-SH AND SI-SH ELECTRODES AND IL AND LP30 ELECTROLYTE

The parameters required to obtain an accurate electrochemical model are derived by the characterization of the battery components. In this section, an overview of the tests for the electrodes and electrolytes is provided.

3.1 METHODOLOGY

3.1.1 CELL ASSEMBLY

Different types of cells were constructed for the electrochemical characterization, as shown in Figure 2. All cells were assembled in an Ar-filled glove box (< 0.1 ppm O_2, < 0.5 ppm H_2O). the different configurations and materials are listed below:

- Full monolayer pouch cell, Figure 2a.: working electrode consists of one-sided coated self-healing NMC811 cathode material punched with a high precision cutter (40 x 50 mm) and the counter electrode consists of one-sided self-healing Si anode material (42 x 52 mm), the electrodes are separated by a glass fiber separator (Whatman GF/D, 45 x 55 mm) and wetted with 1.5 mL of ionic liquid (IL = 1.3 M LiTFSI-PYR_{14}TFSI).
- Full multilayer pouch cell, Figure 2b.: multilayered pouch cells are obtained through stacking N unit cells of the monolayer pouch cell in the following pattern: single-layered anode + separator + double-layered cathode + separator + double-layered anode + … + double-layered cathode + separator + single-layered anode. The 140 mAh pouch cells consist of 3 unit cells with a glass fiber separator, and are wetted with 10 mL IL. The 500 mAh full multilayer pouch cell contains 11 unit cells with a Celgard 2500 separator wetted with 5 mL LP30 (1.2 M $LiPF_6$ in 3:7 w/w EC/DEC from Sigma-Aldrich).
- Half coin cell (CR2032), Figure 2c.: working electrode consists of one-sided coated NMC811-SH cathode or Si-SH anode punched with a precision cutter at a diameter of 15 mm and 16 mm, respectively. The counter electrode consists of Li-foil with a diameter of 16 mm. As half coin cells were only assembled to study the intrinsic properties of the electrodes, the used electrolyte was commercial LP30. Celgard 2500 separator (diameter of 18 mm) was wetted with 40 µL commercial electrolyte: Gotion LP30 (1M $LiPF_6$ - EC:DEC (1:1)).
- Symmetrical coin cells, Figure 2d.: symmetrical cells have been assembled with stainless steel blocking electrodes with a diameter of 16 mm combined with a glass fiber separator and 200 µL IL (1.3 M LiTFSI-PYR_{14}TFSI) or Celgard 2500 and 100 µL LP30 (1.2 M $LiPF_6$ in 3:7 w/w EC/DEC from Sigma-Aldrich).

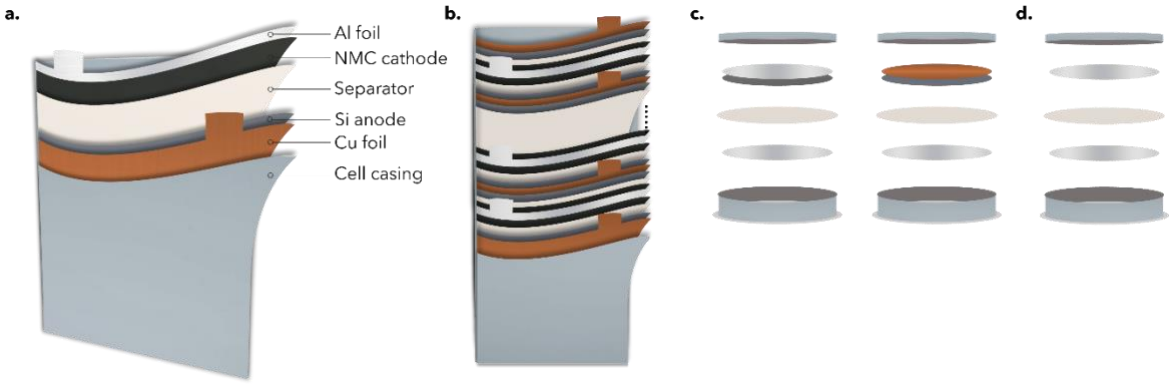

Figure 2: Tested cell configurations for the validation of the electrochemical model and the characterization of the input parameters: a. monolayer pouch cell, b. multilayer pouch cell, c. half coin cells, and d. symmetrical coin cell.

3.1.2 MEASUREMENT TECHNIQUES

Quasi Open Circuit Potential (qOCP)

qOCP is used to obtain the OCP depending on different states of charge (SOC). qOCP is obtained for both electrodes using the half coin cell configuration. As qOCP requires cycling at very slow rates to remain close to equilibrium, currents equivalent to C/25 have been applied.

Electrochemical Impedance Spectroscopy (EIS)

EIS is used to identify the exchange current density, tortuosity, and solid-state diffusion coefficient of the electrodes; and the ionic conductivity and diffusion coefficient of the electrolyte. To obtain the electrode parameters, half coin cells containing Si-SH or NMC811-SH were used. The impedance spectra of the electrodes are obtained with a Gamry 3000 Potantiostat/Galvanostat analyzer by applying a frequency range of 1 MHz - 100 mHz with an 50 mV amplitude. The resulting Nyquist plots are fitted using the Gamry Echem Analyst Software.

In addition, EIS is used to determine the ionic conductivity and diffusion coefficient of the electrolytes. Therefore, a frequency range of 1 MHz – 10 Hz with an 50 mV amplitude are applied on symmetrical coin cells containing SS blocking electrodes and IL+GF or LP30+Celgard 2500, using Bio-Logic VSP electrochemical workstation. The obtained Nyquist plots are fitted using the Z-fit EC-lab Software.

3.2 PARAMETRIZATION RESULTS

3.2.1 qOCP

The OCV vs SOC curve for both electrode materials are obtained by using the qOCP methodology and measure OCV every 5% SOC.

To determine the 5% SOC steps the first charge/discharge cycle of the half coin cells are used. Charging of the NMC cathode shows a capacity of 2.76 mAh with an active material loading of 12.24 mg resulting in a practical capacity of 225.44 mAh/g, meaning that 5% SOC corresponds to steps of 11.27 mAh. Discharging of the NMC cathode has a practical capacity of 178.62 mAh/g, thus 5% SOC corresponds to 8.93 mAh steps.

Employing the same approach for the Si anode. The charging of Si anode exhibits a practical capacity of 3480 mAh/g, resulting in 174 mAh step for 5% SOC. The discharging of Si anode presented a practical capacity of 3576 mAh/g, meaning that 5% SOC corresponds to 179 mAh steps. The obtained OCV vs SOC curves for charging and discharging steps are represented in Figure 3.

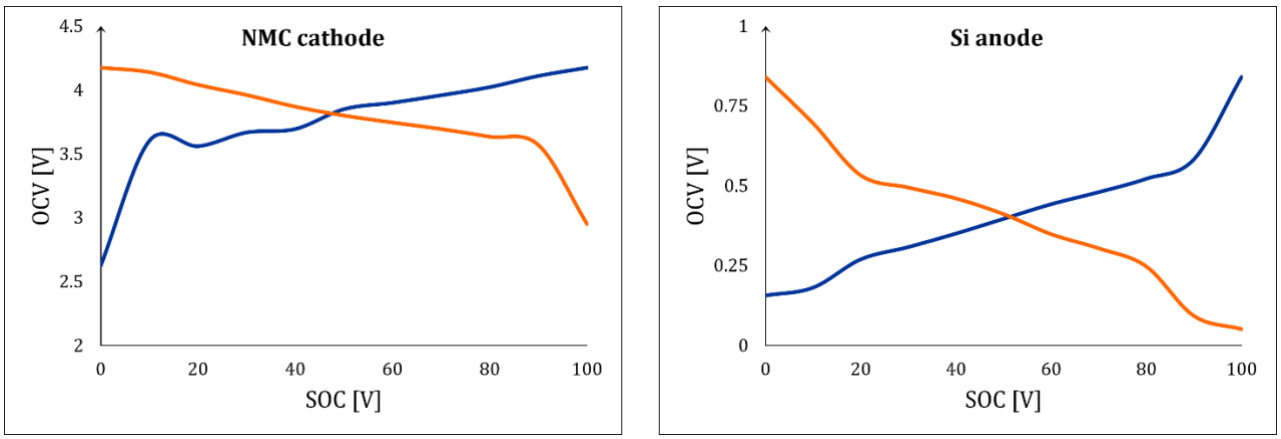

Figure 3: OCV vs. SOC curves for discharging (orange) and charging (blue) NMC cathode and the Si anode, obtained by using the qOCP methodology and measuring OCV every 5% SOC.

3.2.2 EIS

Electrochemical impedance spectroscopy measurement of NMC811-SH polymer cathode and Si-SH polymer anode were performed with specific parameters defined in 3.1.2 on half coin cell configuration, the obtained Nyquist plot is shown in Figure 4. The equivalent circuit shown in Figure 5 was applied to each impedance measurement to find the resistivity of each electrode. R_b represents the bulk resistance of the half-cell, R_{sei} represents the formed SEI of the anode electrode, R_{ct} represents the charge transfer resistance of the electrode, C_{sei} and C_{ct} represent the capacitive effect between SEI-electrolyte and electrode-electrolyte, respectively. The application of the equivalent circuit model through EIS measurement results is given in Table 2.

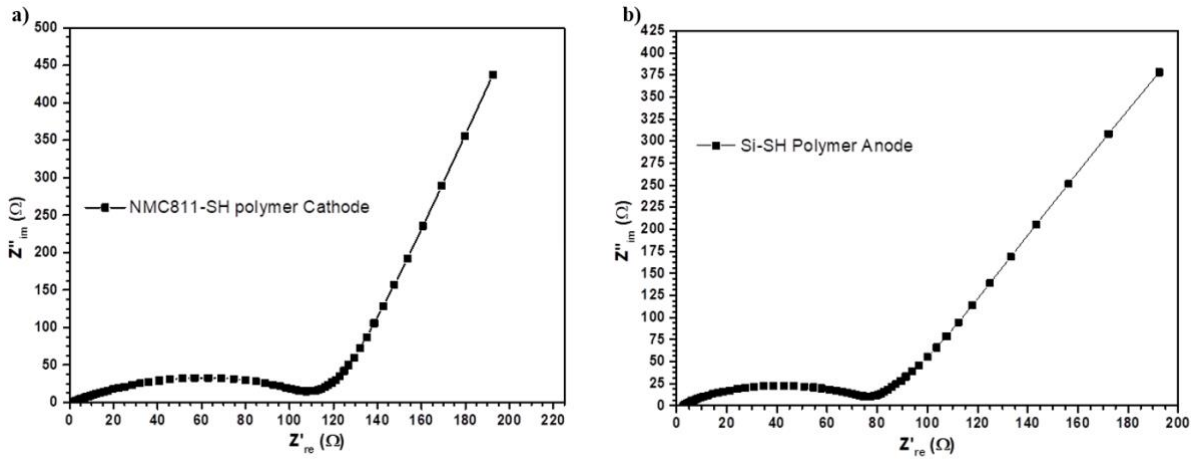

Figure 4: EIS results of a) NMC811-SH polymer cathode, b) Si-SH polymer anode

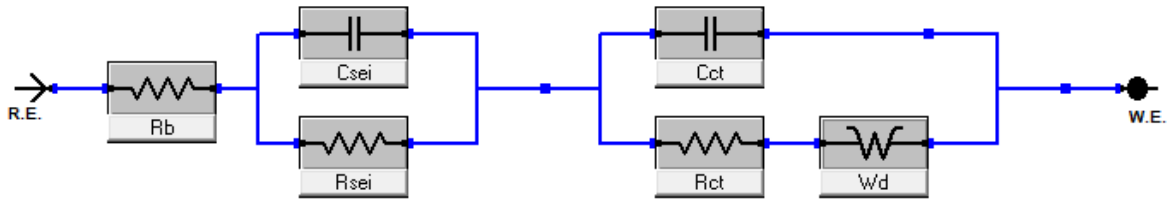

Figure 5: Equivalent Circuit used to fit the impedance measurements

Table 2: EIS results of half coin cells containing NMC811-SH polymer Cathode and Si-SH Polymer Anode via Equivalent circuit model

	Parameter	Value	± Error	Units
NMC811-SH polymer Cathode	R_b	2,173	2,67E-02	Ω
	W_d	4,30E-03	5,60E-05	$Ω/s^{1/2}$
	R_{ct}	10,66	2,12E-01	Ω
	C_{ct}	4,63E-07	7,60E-09	F
	R_{sei}	66,65	6,64E-01	Ω
	C_{sei}	2,84E-06	5,18E-08	F
Si-SH polymer Anode	R_b	3,158	3,12E-02	Ω
	W_d	4,93E-03	6,06E-05	$Ω /s^{1/2}$
	R_{ct}	9,244	3,01E-01	Ω
	C_{ct}	9,81E-07	2,07E-08	F
	R_{sei}	45,05	5,31E-01	Ω
	C_{sei}	3,63E-06	9,54E-08	F

The obtained Nyquist plot from the EIS measurements on the electrodes can be used to obtain the solid diffusion coefficient and the exchange current density.

The solid diffusion coefficient can be obtained through the Warburg coefficient:

$$D = \frac{(RT)^2}{2\,(A\,n^2\,F^2\,c\,\sigma)^2} \tag{8}$$

Where R is the universal gas constant, T the temperature in K, A the working area of the electrode (1,76 cm² for the NMC811 cathode and 2 cm² for the Si anode), n the electron transport ratio of the redox process (equal to 1), F the Faraday constant, c the concentration of Li-ions in the electrode (0.049 mol/cm³ for NMC811 and 0.278 mol/cm³ for Si), and σ the Warburg coefficient (0.0043 Ω/s$^{1/2}$ for NMC811 and 0.0049 Ω/s$^{1/2}$ for Si). Resulting in a solid diffusion coefficient of 2.46 × 10^{-7} cm²/s for NMC811 and 4.72 × 10^{-9} cm²/s for Si.

The exchange current density is obtained through fitting the Nyquist data to an equivalent circuit:

$$i_0 = \frac{RT}{A\,n\,F\,R_{ct}} \tag{9}$$

With R_{ct} the charge-transfer resistance (10.66 Ω for NMC811 and 9.24 Ω for Si), resulting in an exchange current density of 1.34 × 10^{-3} A/cm² for NMC811 and 1.39 × 10^{-3} A/cm² for Si.

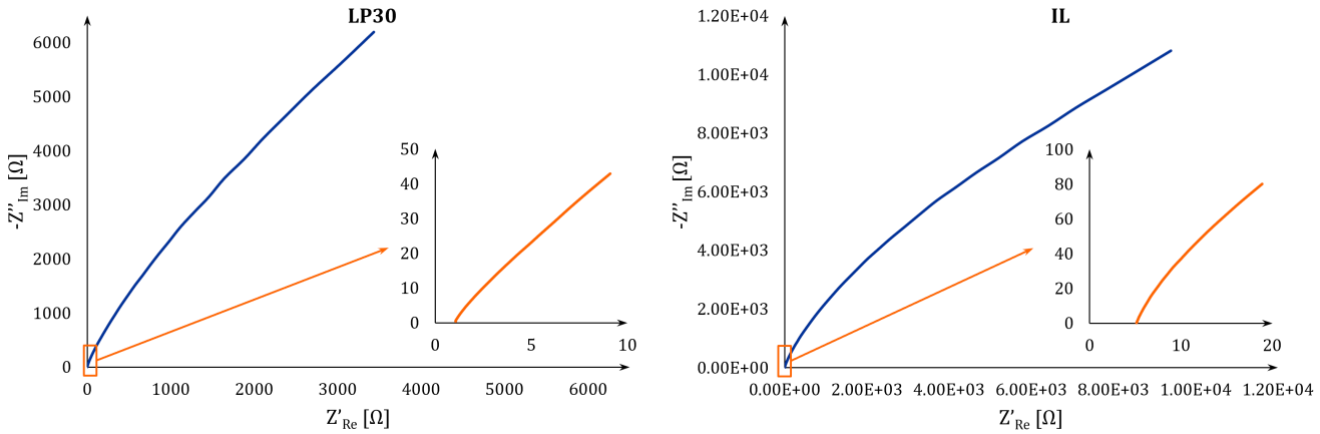

Figure 6: Nyquist plots obtained from the EIS measurements performed on symmetrical coin cells with a detailed view to determine the Rsol as the intercept with the Real impedance axis.

The EIS measurements executed on the electrolyte can be used to obtain the ionic conductivity and thus also the Li-ion diffusion coefficient, the obtained Nyquist plots are provided in Figure 6. After fitting of the Nyquist plot, the ionic conductivity of both electrolyte types can be obtained via:

$$\kappa = \frac{l}{R_{sol}A} \tag{10}$$

With R_{sol} the solution resistance of 1.10 Ω for LP30 and 5.30 Ω for IL, l the thickness of the separator (0.003 cm), and A the area of the separator (2.54 cm²). Obtaining ionic conductivity

values of 1.08×10^{-3} S/cm for LP30 and 2.23×10^{-4} S/cm for IL. The Einstein relation can then be used to obtain the diffusion coefficient of the electrolyte from the ionic conductivity:

$$D = \frac{\kappa\, k_B\, T}{e^2 N_A\, c} \tag{11}$$

With k_B the Boltzmann constant, e the elementary charge, N_A the Avogadro constant and c the lithium-ion concentration within the electrolyte. Diffusion coefficients of 2.39×10^{-7} cm²/s for LP30 and 4.56×10^{-8} cm²/s for IL are obtained.

3.2.3 OVERVIEW OF INPUT PARAMETERS

The obtained parameters are summarized in Table 3.

Table 3: Obtained physical and geometrical parameters to be implemented in the P2D model

Parameter	NMC811	LP30 + CG	IL + GF	Si
Thickness, δ [µm]	65	30	30	36
Initial porosity, ε	0.41			0.83
Inactive part	0.15	-	-	0.4
Particle radius, r_p [nm]	200	-	-	30-50
Electronic conductivity, σ [S m^{-1}]	5.961×10^{-2}	-	-	8.303×10^{-6}
Maximum Li concentration of electrodes, $c_{s,max}$ [mol m^{-3}]	49000	-	-	278000
Diffusivity of solid active material, D_s [cm² s^{-1}]	2.46×10^{-7}	-	-	4.72×10^{-9}
Exchange current density, j_0 [A m^{-2}]	1.34×10^{-3}	-	-	1.39×10^{-3}
Initial electrolyte concentration, $c_{e,0}$ [mol m^{-3}]	-	1200	1300	-
Electrolyte diffusivity, D_e [cm² s^{-1}]	-	2.39×10^{-7}	4.56×10^{-8}	-
Electrolyte conductivity, κ [S cm^{-1}]	-	1.08×10^{-3}	2.23×10^{-4}	-

4. ELECTROCHEMICAL MODELING RESULTS AND VALIDATION

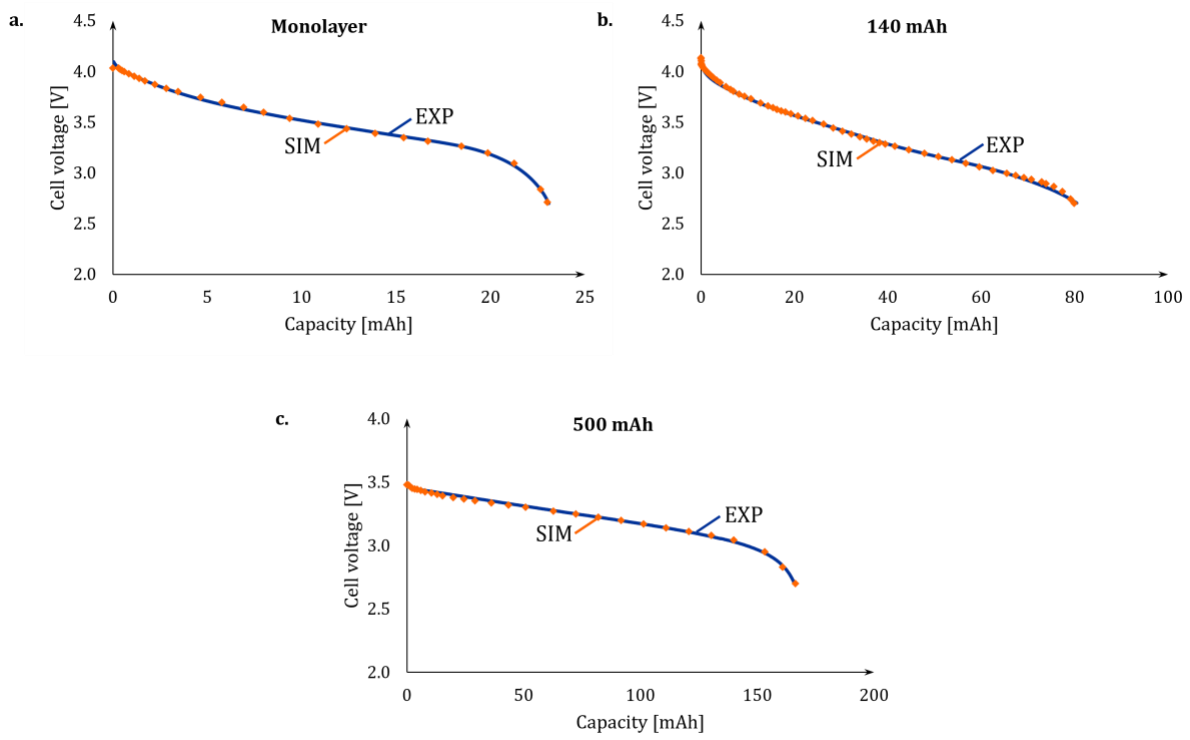

Figure 7: Comparison between experimental and simulated results of a. monolayer pouch cell, b. 140 mAh multilayered pouch cell and c. 500 mAh multilayered pouch cell.

Comparison of the experimental and simulated voltage profiles is depicted in Figure 7. The figure illustrates that the model accurately represents the C/10 discharge behaviour of both Si-SH|IL|NMC811-SH and Si-SH|LP30|NMC811-SH pouch cells. Root-mean-square error (RMSE) values, detailed in Table 4, reinforce the validation of the model, with values below 20 mV. These small variances indicate the model's accurate estimation of battery performance. Notably, Figure 7 demonstrates that the aimed capacities for the multilayered pouch cells where not reached. The models indicate that this stems from the initial capacity of the electrode materials. The initial electrode loading plays a crucial role in determining various aspects of battery performance, including capacity and voltage characteristics (as observed in the model), cycle life, rate capability and coulombic efficiency. For instance, according to the modeling framework for the 500 mAh pouch cells, it is indicated that initially only 50 % of the total capacity of the cathode and 45 % of the total capacity of the anode are utilized. Optimizing electrode loading during battery manufacturing is essential for achieving desired performance metrics.

Scaling up the models from monolayer coin cell to a 500 mAh pouch cell suggests that the modeling parameters established for a small-scale cell can effectively predict the discharge

behaviour of a larger multilayered pouch cell without requiring further adjustments. This capability enables the prediction of the effects of upscaling on specific cell configurations.

Table 4: RMSE between experimental and simulated results for monolayer and multilayered pouch cells.

Cell configuration		RMSE [mV]
Monolayer	Si-SH | IL | NMC811-SH	15.8
140 mAh	Si-SH | IL | NMC811-SH	18.2
500 mAh	Si-SH | LP30 | NMC811-SH	10.4

The observed non-ideal behaviour, characterized by a voltage drop in the discharge curves, is attributed to polarization. Generally, discharge curves can be categorized into three regions, each dominated by a specific cause of polarization. At the beginning of discharge, an abrupt voltage decline is noticeable. This immediate reduction in voltage results from Ohmic polarization, stemming from the flow of current across internal resistance, thus affecting charge transfer within the battery system. According to Ohm's law, increasing the applied C-rate amplifies the polarization tendency of the battery.

The gradual voltage decrease observed in the plateau zone is attributed to activation polarization, which is associated with the kinetics of electrochemical reactions. This involves the necessary overpotential to surmount the activation energy barrier at the electrode/electrolyte interface, a phenomenon described by the Butler-Volmer equation. Conversely, the abrupt voltage drop observed towards the end of discharge stems from concentration polarization, arising from resistance encountered during the mass transfer process. This occurs because electrochemical reactions consume reactants faster than they diffuse into the porous electrode, leading to a depletion of Li-ions and consequently a decrease in their concentration. The resulting difference in Li-ion concentration between the bulk electrolyte and the electrode induces a reduction in local potential near the cathode. During the initial phase of discharge, concentration polarization is minimal, but it escalates rapidly towards the discharge's conclusion and with increasing C-rates.[11,12]

The simulations show minimal deviations from the experimental results, possibly due to two factors. Firstly, the P2D geometry of the model assumes negligible gradients of variables parallel to the current collectors and near the tabs, thus overlooking potential drops due to polarization. Hence, employing a two- or three-dimensional geometry could prove advantageous.[13] Secondly, the model assumes homogeneous components, disregarding variations in particle radii within electrodes, resulting in a uniform potential distribution and potentially missing the polarization effect.[11] Possible optimizations in modeling may involve

incorporating film resistance, considering particle size distribution, and accounting for the non-spherical nature of electrode particles.

5. CONCLUSION

Deliverable D4.6 summarizes the activities for the development of an electrochemical modeling framework designed to forecast the behaviour of self-healing electrodes and ionic liquid electrolytes. At first, battery components where experimentally characterized to obtain accurate input parameter integration into the models. Thereafter, the model was developed at monolayer pouch cell level, including the optimization and experimental validation of the simulations. Afterwards the framework is extended to multilayered pouch cells.

The discharge experiments validate the models at different models, demonstrating high accuracy across various cell configurations. Upscaling the modeling framework does not require additional characterization of cell components. This characteristic facilitates the prediction of the upscaling effect for a specific cell configuration without necessitating extra experimental efforts, thus substantially reducing the development time for new battery configurations.

REFERENCES

[1] Wang J, Meng J, Peng Q, Liu T, Zeng X, Chen G, et al. Lithium-Ion Battery State-of-Charge Estimation Using Electrochemical Model with Sensitive Parameters Adjustment. Batteries 2023;9. https://doi.org/10.3390/batteries9030180.

[2] Liu K, Gao Y, Zhu C, Li K, Fei M, Peng C, et al. Electrochemical modeling and parameterization towards control-oriented management of lithium-ion batteries. Control Eng Pract 2022;124. https://doi.org/10.1016/j.conengprac.2022.105176.

[3] KREMER F, RAEL S, URBAIN M. 1D electrochemical model of lithium-ion battery for a sizing methodology of thermal power plant integrated storage system. AIMS Energy 2020;8:721–48. https://doi.org/10.3934/energy.2020.5.721.

[4] Sarkar S, Zohra Halim S, El-Halwagi MM, Khan FI. Electrochemical models: methods and applications for safer lithium-ion battery operation. J Electrochem Soc 2022;169:100501. https://doi.org/10.1149/1945-7111/ac8ee2.

[5] Doyle M, Newman J. Comparison of Modeling Predictions with Experimental Data from Plastic Lithium Ion Cells Acknowledgment. J Electrochem Soc 1996;143:1890–903.

[6] Xia L, Najafi E, Bergveld HJ, Donkers MCF. A Computationally Efficient Implementation of an Electrochemistry-Based Model for Lithium-Ion Batteries. IFAC-PapersOnLine 2017;50:2169–74. https://doi.org/10.1016/j.ifacol.2017.08.276.

[7] Petit M, Calas E, Bernard J. A simplified electrochemical model for modelling Li-ion batteries comprising blend and bidispersed electrodes for high power applications. J Power Sources 2020;479:228766. https://doi.org/https://doi.org/10.1016/j.jpowsour.2020.228766.

[8] Smekens J, Paulsen J, Yang W, Omar N, Deconinck J, Hubin A, et al. A Modified Multiphysics model for Lithium-Ion batteries with a LixNi1/3Mn1/3Co1/3O2 electrode. Electrochim Acta 2015;174:615–24. https://doi.org/10.1016/j.electacta.2015.06.015.

[9] Comsol. The Battery Design Module User's Guide. 2020.

[10] Xia B, Zhao X, de Callafon R, Garnier H, Nguyen T, Mi C. Accurate Lithium-ion battery parameter estimation with continuous-time system identification methods. Appl Energy 2016;179:426–36. https://doi.org/10.1016/j.apenergy.2016.07.005.

[11] Mei W, Liang C, Sun J, Wang Q. Three-dimensional layered electrochemical-thermal model for a lithium-ion pouch cell. Int J Energy Res 2020;44:8919–35. https://doi.org/https://doi.org/10.1002/er.5601.

[12] Qiu C, He G, Shi W, Zou M, Liu C. The polarization characteristics of lithium-ion batteries under cyclic charge and discharge. Journal of Solid State Electrochemistry 2019;23:1887–902. https://doi.org/10.1007/s10008-019-04282-w.

[13] Kim US, Shin CB, Kim C-S. Modeling for the scale-up of a lithium-ion polymer battery. J Power Sources 2009;189:841–6. https://doi.org/https://doi.org/10.1016/j.jpowsour.2008.10.019.